Large collective motions regulate the functional properties of glutamate transporter trimers

Jie Jiang[a,b], Indira H. Shrivastava[c], Spencer D. Watts[a], Ivet Bahar[c], and Susan G. Amara[a,b,1]

[a]Department of Neurobiology, [b]Center for Neuroscience, and [c]Department of Computational and Systems Biology, School of Medicine, University of Pittsburgh, Pittsburgh, PA 15261

Contributed by Susan G. Amara, July 26, 2011 (sent for review April 1, 2011)

Glutamate transporters clear synaptically released glutamate to maintain precise communication between neurons and limit glutamate neurotoxicity. Although much progress has been made on the topology, structure, and function of these carriers, few studies have addressed large-scale structural motions collectively associated with substrate transport. Here we show that a series of single cysteine substitutions in the helical hairpin HP2 of excitatory amino acid transporter 1 form intersubunit disulfide cross-links within the trimer. After cross-linking, substrate uptake, but not substrate-activated anion conductance, is completely inhibited in these mutants. These disulfide bridges link residue pairs >40 Å apart in the outward-facing crystal structure, and can be explained by concerted subunit movements predicted by the anisotropic network model (ANM). The existence of these global motions is further supported by the observation that single cysteine substitutions at the extracellular part of the transmembrane domain 8 can also be cross-linked by copper phenanthroline as predicted by the ANM. Interestingly, the transport domain in the un-cross-linked subunit of the trimer assumes an inward-facing orientation, suggesting that individual subunits potentially undergo separate transitions between outward- and inward-facing forms, rather than an all-or-none transition of the three subunits, a mechanism also supported by ANM-predicted intrinsic dynamics. These results shed light on how large collective motions contribute to the functional dynamics of glutamate transporters.

Neuronal and glial excitatory amino acid transporters (EAATs) function to clear glutamate from the extracellular (EC) space during neurotransmission, thus enabling precise excitatory signaling. Glutamate transport also limits the neuronal death that can be triggered by excess EC glutamate (1). These carriers belong to a secondary active transporter family that utilizes the driving force stored in ion electrochemical gradients to enable the uphill translocation of their substrates (2, 3). In addition, EAATs mediate a thermodynamically uncoupled anion flux (4, 5), which has been proposed to serve as a feedback sensor to reduce cell excitability (6).

EAATs are thought to function through an alternating access mechanism, in which the structure alternates between outward- and inward-facing states to expose the substrate-binding site to either EC or intracellular (IC) environments (7). Our understanding of this mechanism has been greatly expanded by structural and functional studies of prokaryotic and mammalian glutamate transporters (for a review, see ref. 8) and by several high-resolution structures of an archaeal ortholog, Glt_{Ph} (9–11). Glutamate transporters are trimers comprised of identical subunits containing two domains: an N-terminal domain with six transmembrane (TM) α-helices, also referred to as the trimerization domain, and a C-terminal transport domain containing essential binding sites for substrate and cotransported ions. The transport domain is comprised of two opposite-facing helical hairpins (HP1 and HP2), a helix interrupted by a β-linker (TM7) and an amphipathic helix (TM8).

The two helical hairpins, HP1 and HP2, cradle the substrate-binding site, and have been proposed to act as inner and outer gates, respectively (9). During transport, substrates and cotransported ions alter the solvent accessibility of HP2, implying that the region undergoes conformational changes (12, 13). Molecular dynamics (MD) simulations revealed that the HP2 loop possesses an intrinsic, structure-induced ability to open up, exposing the substrate-binding site to the aqueous basin, and to close down after substrate and sodium binding, thus acting as an EC gate (14). Several studies also support the idea that conformational changes in HP1 are required to release substrate intracellularly. Residues at the HP1 loop are accessible to water and hydrophilic agents from both sides of the membrane (15), and it has been proposed that the inward movement of HP1 results in the opening of a pathway between the binding pocket and the cytoplasm (16).

In addition to these local opening and closing motions associated with HP1 and HP2, a recent crystal structure of Glt_{Ph} captures an inward-facing state of the transporter in which the C-terminal transport domain of each subunit has moved approximately 18 Å toward the cytoplasm [Protein Data Bank (PDB) ID 3KBC] (11). This large-scale movement, also consistent with computational predictions (17), exposes the transport domain to the IC environment and predisposes the structure to release the bound substrate to the cytoplasm. Thus, local conformational changes of HP1 and HP2 allow for the opening or occlusion of the substrate-binding site, whereas the movement of the transport domain provides a means for transition between outward- and inward-facing states. Whether other large-scale movements exist and regulate carrier functions remains to be elucidated.

In the present study, we use cysteine cross-linking and computational analyses to identify a series of large-scale collective motions that are intrinsic to glutamate transporter trimers. These collective motions are functionally important for substrate transport, but not the substrate-gated anion conductance. Furthermore, we show that these collective motions are coupled to the inward movement of the transport domain, and thus serve a critical function to enable alternating access.

Results

Inhibition of Substrate Transport by Copper Phenanthroline (CuPh) in Single Cysteine Substitution Mutants in HP2b. We previously used CuPh-catalyzed cross-linking of cysteine pairs introduced into a highly functional cysteineless version of human EAAT1 (CSLS) to show the critical roles of HP2 in initial substrate binding and HP1 in later translocation steps (18). Unexpectedly, treatment of a single cysteine mutant, V449C, with CuPh (300 μM) for 5 min abolishes transport activity at both low (5 μM) (Fig. 1*A*) and high (up to 1 mM, Fig. S1*A*) L-glutamate concentrations. More surprisingly, further treatment of the CuPh-treated V449C with 20 mM DTT to reduce disulfide bonds not only recovers, but also increases substrate transport, suggesting these bonds form

Author contributions: J.J., I.H.S., S.D.W., I.B., and S.G.A. designed research; J.J. and I.H.S. performed research; J.J., I.H.S., S.D.W., I.B., and S.G.A. analyzed data; and J.J., I.H.S., I.B., and S.G.A. wrote the paper.

The authors declare no conflict of interest.

[1]To whom correspondence should be addressed. E-mail: amaras@pitt.edu.

This article contains supporting information online at www.pnas.org/lookup/suppl/doi:10.1073/pnas.1112216108/-/DCSupplemental.

spontaneously (Fig. 1*A*). Indeed, treatment with DTT alone also enhances the transport activity of V449C. V449C readily forms these cross-links with a second-order rate constant of 1,790± 262.8 M^{-1} s^{-1}. Moreover, Cd^{2+} (100 μM), which can coordinate thiol groups of cysteine residues in close proximity (19), significantly inhibits the transport activity of V449C (Fig. 1*A*). We also explored the effect of CuPh on the mutant I453C, a residue one helical turn away from V449. CuPh (300 μM) significantly inhibits the uptake activity of I453C (approximately 50%, Fig. 1*B*). The remaining transport activity appears to arise from un-cross-linked I453C, because additional treatment with a thiol-modifying reagent, 2-(trimethylammonium)ethyl] methanethiosulfonate bromide (MTSET), or prolonged incubation with CuPh further reduces its activity (Fig. S1*B*). The inhibition of I453C by CuPh can be completely reversed by DTT, but no enhancement of transport activity is seen as for V449C (Fig. 1*B*).

Residues V449 and I453 are located at the N terminus of helix HP2b, which along with HP2a forms the helical hairpin HP2 (Fig. 1*C*). Examination of cysteine substitutions near the HP2 loop demonstrates that several residues in this region readily form disulfide bonds. Upon treatment with CuPh, the uptake activity of L448C is also completely inhibited (Fig. 2*A*). Furthermore, DTT treatment not only recovers, but also significantly increases transport activity of this mutant, to an even greater degree than it does for V449C (Fig. 2*B*). In contrast, substrate transport by carriers with mutations near the C terminus of HP2b (L455C, T456C, and V458C) is not inhibited by CuPh, indicating that they do not achieve sufficient proximity to form disulfide bonds.

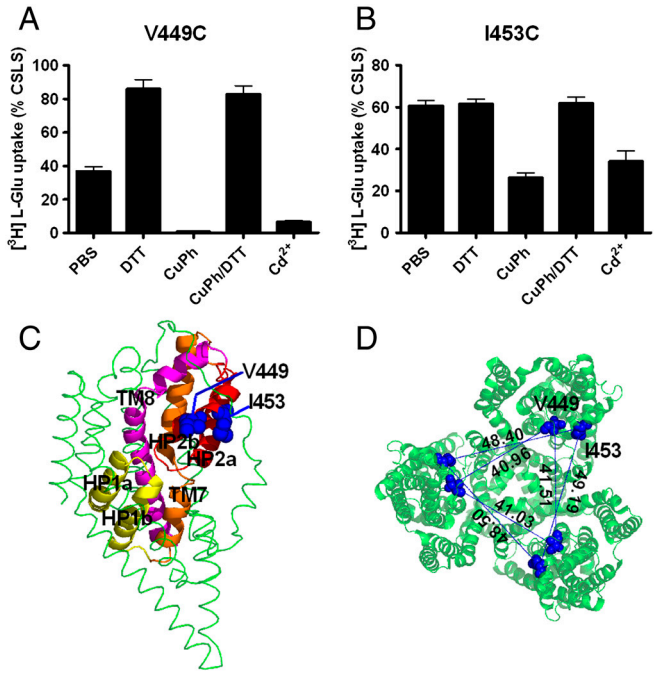

Fig. 1. Inhibition of substrate transport by CuPh and cadmium in mutants V449C and I453C. COS7 cells were treated with 20 mM DTT, 300 μM CuPh, or CuPh followed by DTT, for 5 min. For CuPh preparation, $CuSO_4$ and 1,10-phenanthroline were mixed in a 1:2 ratio prior to use. Uptake assays were performed for 10 min at room temperature using 5 μM L-[^{3}H] glutamate as substrate. The effect of cadmium on transport activity was determined by including 100 μM cadmium chloride in the uptake solution. Data for V449C (*A*) and I453C (*B*) are expressed as the percent of uptake activity relative to the CSLS control. (*C*) Locations of V449 and I453 on the helix H2b of the HP2 hairpin, shown for one subunit (side view). (*D*) Estimated distances between the three V449 residues, and the three I453 residues in an EAAT1 trimer (top view). The illustrations are based on the Glt_{Ph} crystal structure in the outward-facing state (PDB ID 1XFH) and are made using the software Pymol.

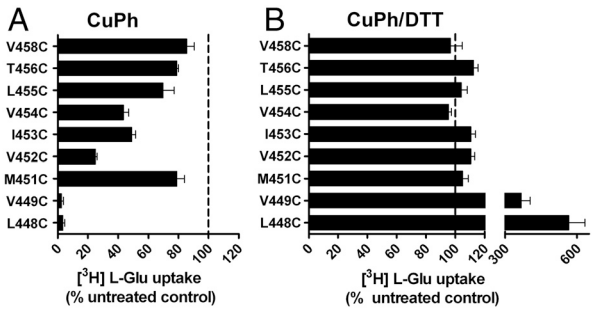

Fig. 2. Single cysteine substitutions at the N terminus of the helix HP2b are more reactive and form spontaneous cross-links. (*A*) The effects of 300 μM CuPh on the L-glutamate transport activity of a series of cysteine substitution mutants. (*B*) Substrate transport by mutant transporters after addition of 20 mM DTT for 5 min. Uptake assays were performed as described in Fig. 1 and data are represented as the percentage of untreated controls in two to four experiments done in triplicate.

CuPh Induces Cross-Linking Between Two Subunits in the Same Trimer. Because V449C and I453C contain only one cysteine per subunit within the trimers, the disulfide bridges observed must span two subunits (Fig. 1*D*), and should be readily detectable as dimers by nonreducing SDS-PAGE. We employed *Xenopus* oocytes for this experiment because EAATs tend to migrate as oligomers on polyacrylamide gels when overexpressed in COS7 cells. In oocytes, CuPh and DTT have similar effects on the uptake activity of V449C and I453C as in COS7 cells (Fig. 3). When analyzed by nonreducing SDS-PAGE, CSLS transporters migrate as two species at a molecular mass of approximately 70 and 50 kDa, corresponding to fully glycosylated and unglycosylated/partially glycosylated monomers, respectively. With V449C and I453C, an additional approximately 140 kDa species appears upon treatment with CuPh, consistent with the predicted size of a cross-linked dimer. This high molecular weight band disappears when V449C-expressing oocytes are further incubated with DTT. The mutant I453C shows a stronger dimer-band signal compared to V449C, although transport by I453C is less dramatically inhibited after cross-linking (Fig. 3). Additional experiments revealed that the V449C cross-links are less stable during oocyte membrane pre-

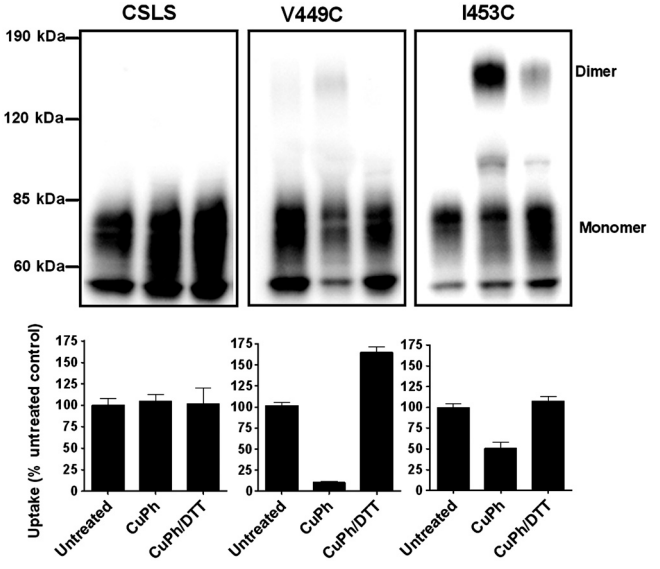

Fig. 3. CuPh-induced cross-linking occurs between two subunits. Transporters were expressed in *Xenopus* oocytes and treated as indicated. Oocyte membranes were lysed and separated by nonreducing gradient SDS-PAGE and subjected to Western blotting analyses. Uptake assays in oocytes were carried out at room temperature using 5 μM L-[^{3}H] glutamate as substrate for 15 min, and data are normalized to untreated controls.

paration, because we observed a similar inhibition of uptake, but a substantially more prominent V449C dimer species using a bifunctional cross-linker (1,8-octadiyl bismethanethiosulfonate, M8M) instead of CuPh (Fig. S2). We also ruled out that the cross-linking might take place between a transporter subunit and an unknown protein of similar size (Fig. S3), or between subunits from two adjacent trimers (Fig. S4). Overall, our results strongly suggest that V449C and I453C form CuPh-catalyzed, DTT-reversible disulfide bonds between two transporter subunits within a single trimer.

Anisotropic Network Model (ANM) Analysis Suggests That Large Collective Motions in the Trimer Can Significantly Alter Intersubunit Distances. The α-carbons of V449 and I453 are separated by >40 Å in the outward-facing structure of Glt_{Ph} (PDB ID 1XFH) (Fig. 1*D*) and by >30 Å in the inward-facing structure (PDB ID 3KBC), even though they would need to be within 7 Å to form disulfide bonds (20, 21). The observance of intersubunit disulfide bridges suggests that sufficiently large conformational rearrangements take place to bring the HP2b helices of two subunits together. Our recent MD simulations of outward-facing Glt_{Ph} showed that HP2, acting as an EC gate, opens within tens of nanoseconds and displaces the HP2 loop approximately 10 Å toward the central basin (14). In light of experimental data showing the propensity of the HP2 loop to form intersubunit cross-links, we reexamined the MD trajectories in Glt_{Ph}, and found that the minimum distance between the α-carbons of I361 residues (V449 in EAAT1, see sequence alignment in Fig. S5) is approximately 30 Å, too great a distance for disulfide bond formation. Clearly, larger movements, outside the range of MD simulations, are required to explain the data. Thus, we turned to ANM analysis (22, 23) to investigate the large collective dynamics of Glt_{Ph}.

ANM analysis allows assessment of the collective fluctuations or so-called global motions that are intrinsically accessible to a given structure under physiological conditions. In this approach, the structure is modeled as a network of harmonic oscillators. The nodes of the network are identified by the α-carbons and the springs, usually taken to be uniform (identical force constants), account for interresidue interactions. The collective dynamics of such a network is uniquely defined by the network topology and resolved by a normal mode analysis into 3*N*-6 modes of motions. The shape and frequency of each mode k is described by the eigenvector $\boldsymbol{u}_k$ and eigenvalue λ_k, respectively (see *SI Materials and Methods*. The top-ranking modes are characterized by low-frequency/large-amplitude movements that generally occur within a micro- to millisecond time range. These so-called softest modes usually play a dominant role in defining the structural changes involved in the biological activity of the protein, as has been demonstrated for both water-soluble and membrane proteins (22–25). In the case of Glt_{Ph}, three softest modes are distinguished by their high collectivity. The first two (modes 1 and 2) are degenerate —i.e., they have same frequency and complement each other. In these modes, two subunits move toward each other, while the third moves outward, and vice versa (Fig. 4*A*). The third (mode 3) is a nondegenerate mode that cooperatively induces a symmetric opening/closing of all three subunits (Fig. S6*A*). We refer to these modes as asymmetric stretching/contraction (modes 1 and 2), and symmetric opening/closing (mode 3). These modes are described in Movies S1–S3. Fig. 4*B* illustrates the potential change in intersubunit distances of residues in HP2 as the molecule would gradually move along the asymmetric stretching/contraction mode. Residues in HP2b, particularly those at the N terminus of the helix, tend to come into close proximity, whereas those at the C terminus remain well separated (Fig. 4*B*), consistent with our experimental data. Similar results were also observed in symmetric mode (Fig. S6*B*). In principle, a multitude of modes simultaneously drive the dynamics of the carrier to bring HP2 domains together, with the softest modes, including the two shown here, providing the largest contributions.

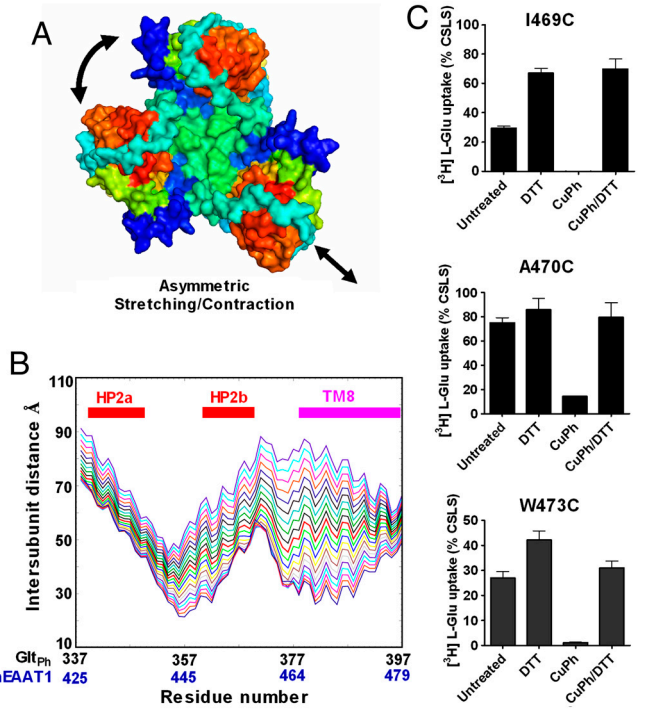

Fig. 4. Large collective motions of glutamate transporters predicted by ANM analysis. (*A*) Schematic representation of the asymmetric stretching/contraction mode viewed from the EC face. The arrows indicate the direction of motion of the three subunits. (*B*) Intersubunit distances of residues in HP2 and TM8 (based on Glt_{Ph} C^{α} atoms between two approaching subunits) are significantly altered along the asymmetric stretching/contraction mode. The thick red curve refers to the equilibrium distances derived from the X-ray structure (PDB ID 1XFH), and the series of curves above and below refer to different extents of deformation along this softest mode in the positive and negative directions. EAAT1 residue numbers are denoted in blue, below the abscissa. (*C*) Inhibition of substrate transport in mutants with single cysteines substituted into the N terminus of TM8. Cross-linking and uptake assays were performed as described in Fig. 1.

Interestingly, the analysis of global motions suggests that residues at the N terminus of TM8 also come into close proximity (Fig. 4*B*). Inspired by this observation, we substituted cysteines for several additional residues in this region and examined the effects of CuPh and/or DTT on transport activity. Fig. 4*C* shows the uptake activity for TM8 mutants I469C, A470C, and W473C. Consistent with the residue proximities predicted by ANM analysis, the transport activity of these mutants is significantly impaired by CuPh, and this inhibition can be reversed by DTT. The second-order rate constants for I469C, A470C, and W473C are 6,375 ± 1,344, 372 ± 116, and 5,882 ± 2094 M^{-1} s^{-1}, respectively. Furthermore, I469C and W473C form spontaneous cross-links, because DTT significantly increases their uptake activity compared to untreated controls. We also observed dimer-band signals in I469C and W473C after treatment with the bifunctional cross-linker M8M (Fig. S2*C*). These data confirm and reinforce the idea that large collective motions of glutamate transporters, consistent with the softest modes predicted by the ANM analysis, underlie the unexpected proximities of residues within the trimer.

The Un-Cross-Linked Subunit of the V449C Trimer Faces Inward. One critical step in the glutamate transport cycle is the inward movement of the transport domain of each subunit, which enables the IC release of substrate and cotransported ions (11). We hypothesized that the large collective motions might be important for the transport domain movement. To test this idea, we focused on the V449C mutant, which exhibits a high propensity to cross-link and

asked whether the un-cross-linked V449C subunit within the trimer is in an outward- or inward-facing state.

In the inward-facing conformation of Glt_{Ph}, distinct sets of residues are accessible to the EC and IC environment (Fig. 5*A*). We first determined whether the V449C residue in the un-cross-linked subunit is accessible by either an irreversible (N-ethylmaleimide, NEM) or a reversible (MTSET) thiol-modifying reagent applied from the outside. Earlier studies have shown that modification of V449C abolishes substrate transport (26). If NEM could modify the V449C residue in the un-cross-linked subunit, uptake activity should be reduced by as much as one-third, assuming the three subunits operate independently as has been proposed (27, 28). Our results showed that V449C-expressing cells sequentially treated with CuPh/NEM/DTT exhibit uptake activity comparable to those treated with CuPh/PBS/DTT or CuPh/MTSET/DTT (Fig. 5*B*), suggesting either that the single free cysteine in the V449C trimer is inaccessible to NEM or that modification in one subunit does not affect trimer function. To exclude the latter possibility, we used a biotin-conjugated thiol-modifying reagent (maleimide-PEO_2-biotin) to react with free cysteines. Although the un-cross-linked V449C carrier can be readily biotinylated and affinity purified, the residue no longer reacts with the maleimide-based biotin reagent after cross-linking (Fig. 5*C*). Thus, V449C in the un-cross-linked subunit is inaccessible to modification reagents, indicating that the un-cross-linked subunit exists in an inward-facing conformation.

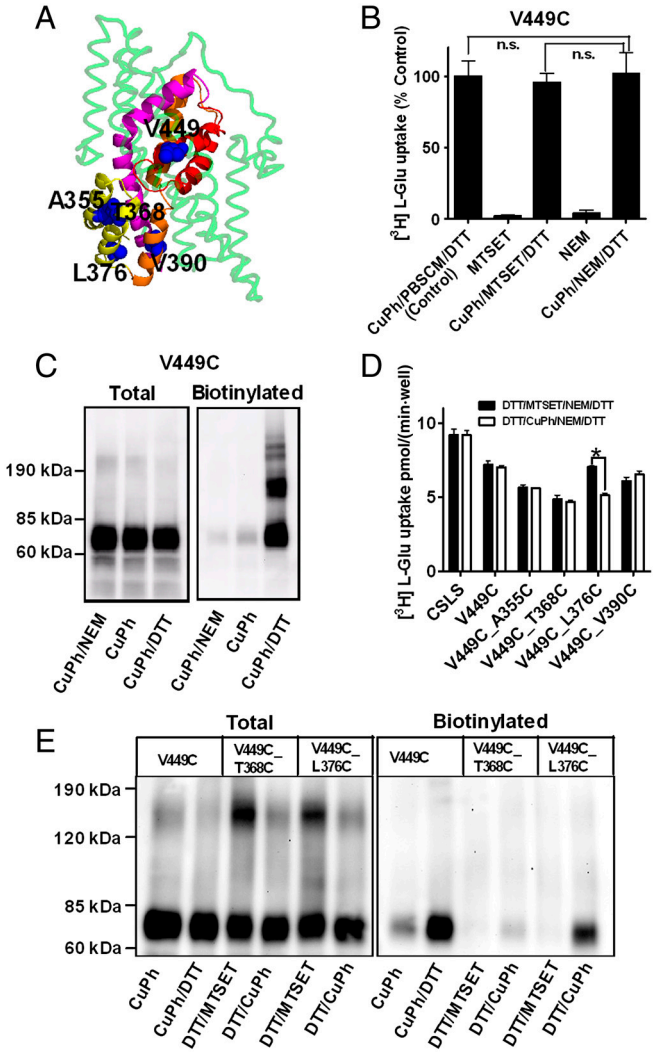

Fig. 5. The un-cross-linked subunit is in inward-facing conformation after V449C cross-linking. (*A*) Location of residues (V449, A355, T368, L376, and V390) in the context of the inward-facing Glt_{Ph} crystal structure (PDB ID 3KBC). (*B* and *D*) COS7 cells were treated for 5 min with 300 μM CuPh, 1 mM MTSET, 0.5 mM NEM, or 10 mM DTT as indicated. Uptake assays were performed as described in Fig. 1. After treatments, surface proteins were biotinylated with maleimide-PEO_2-biotin (*C*) or maleimide-biotin (*E*) and subjected to Western blotting analyses. n.s., not significant; *, $p < 0.05$.

An earlier study reported that several cysteine substitutions in HP1, TM7, and TM8 of a rat glutamate transporter (GLT-1) display increased accessibility to the membrane permeable reagent, NEM, when external sodium was replaced by potassium, a condition expected to increase the proportion of inward-facing transporters (16). Similarly, several equivalent residues in EAAT1 (A355C, T368C, L376C, and V390C) are exposed intracellularly as the transport domain moves toward the cytoplasm (Fig. 5*A* and Fig. S7). We introduced these conformationally sensitive cysteines into the V449C mutant and asked if these residues were accessible intracellularly in the un-cross-linked subunit after V449C cross-linking. As a control, we used the membrane impermeant reagent, MTSET, to protect V449C residues from further modification and to lock transporters in an outward-facing conformation (26). In addition, cells were pretreated with DTT to reverse spontaneous V449C cross-links. We found that transport by V449C_L376C is significantly inhibited after sequential treatment with DTT/CuPh/NEM/DTT when compared with DTT/MTSET/NEM/DTT. Other double mutants (V449_A355C, V449C_T368C, and V449C_V390C) show no differences in substrate transport between the two treatments (Fig. 5*D*). In addition, significant amounts of V449C_L376C can be affinity purified using a membrane-permeable biotin-conjugated thiol-modifying reagent (maleimide-biotin) after cross-linking, but not for the mutant V449C_T368C (Fig. 5*E*). L376C is most proximal to the cytoplasm among the residues tested, and would be the first exposed to the IC environment as the transport domain moves down (Fig. 5*A*). These data confirm that the un-cross-linked subunit is inwardly oriented when the two remaining subunits are cross-linked extracellularly.

Glutamate Transporters Favor Stepwise Transitions Between Outward- and Inward-Facing States. To explore whether all three glutamate transporter subunits tend to undergo an all-or-none allosteric transition between inward- and outward-facing states, typical of the Monod–Wyman–Changeux model or a stepwise transition to enable alternating access, we examined the distribution of ANM modes that contribute to the transition between different states. Fig. 6 *A* and *B* illustrates four possible states and transitions between these states, with the numbers of outward/inward-facing subunits being 3/0, 2/1, 1/2, and 0/3. The states 3/0 and 0/3 are the experimentally resolved Glt_{Ph} structures, and 2/1 and 1/2 are models reconstructed by assembling the outward- and inward-facing subunits. We asked whether the stepwise passage from 3/0 to 0/3 through the 2/1 and 1/2 conformers is more accessible compared to the all-or-none passage between the two end states. The cumulative overlap (described by a 3*N*-dimensional difference vector **d**; see *SI Materials and Methods*) represents the degree to which each subset of modes, starting from the slowest, contributes to the overall structural change between two endpoints, and thus provides a means to compare the ease of different transitions (25). Fig. 6 *C* and *D* displays the contributions of the 50 softest modes (u_k, $1 \leq k \leq 50$) to the forward and reverse transitions around the cycle depicted in Fig. 6*B*. We find that each of the three transitions that involve intermediate states is achieved by fewer number of low-frequency modes (i.e., energetically more favorable) and is thus "easier" than the all-or-none transition. These results support the notion that the intermediate state we observed after cross-linking is a physically viable step toward achieving the fully inward conformation.

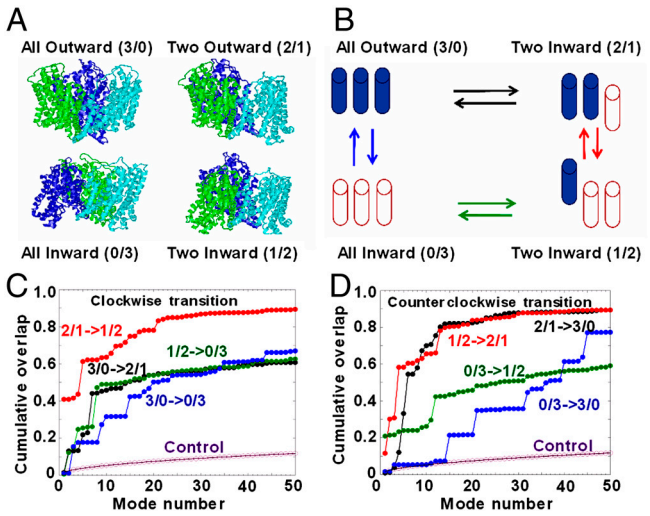

Fig. 6. Cumulative overlap of ANM modes for transitions between pairs of conformations. (*A*) Ribbon diagrams of the four structures used for transport domain transitions. The all-inward (0/3) and all-outward conformations (3/0) represent the 3KBC and 1XFH structures, respectively. In the intermediate structure model designated as 2/1, one subunit faces inward (cyan), whereas in 1/2, two subunits face inward (green and cyan). (*B*) A schematic representation of the passages between different conformations. (*C* and *D*) Cumulative overlap of the ANM modes with the deformation vector between pairs of conformations indicated by the labels on the paths. The control curves refer to the case of randomly oriented modes that contribute equally to conformational transitions.

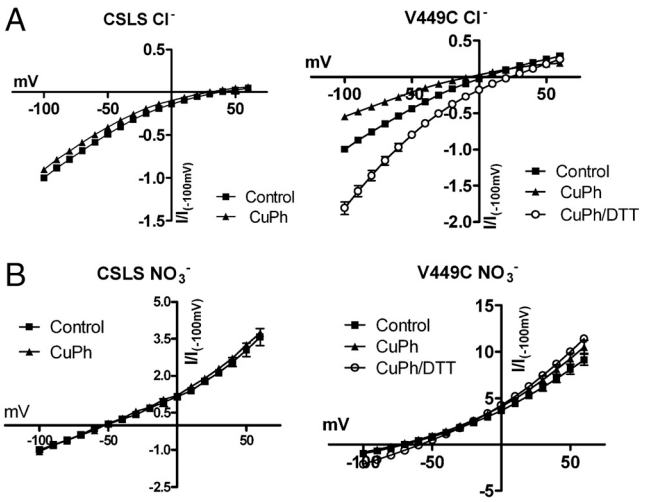

Fig. 7. V449C retains anion conductance after cross-linking. Using a two-electrode voltage clamp, currents from oocytes expressing CSLS or V449C were recorded in normal chloride-containing solution (*A*) and in a solution in which chloride was replaced by NO_3^- (*B*). Recordings were made before (■) and after (▲) application of 300 μM CuPh (5 min), as well as after initial treatment with 20 mM DTT (5 min, ○). The currents obtained in the absence of glutamate were subtracted from those elicited by 1 mM L-glutamate. Currents were normalized to the control currents obtained at −100 mV.

The Substrate-Gated Anion Flux Remains After Cross-Linking. In addition to transporting substrate and cotransported ions, EAATs also function as glutamate-activated anion channels. Thus, glutamate-elicited currents are comprised of a substrate-coupled component that dominates at a membrane potential of −100 mV, and a substrate-uncoupled anion component that dominates at +60 mV. To examine the impact of cross-linking on anion channel activity, we focused on V449C, which displays minimal transport activity after cross-linking in oocytes, thus no substrate-coupled current. In normal chloride solution, CSLS-expressing oocytes exhibit similar glutamate-elicited currents before and after CuPh treatment (Fig. 7*A*). After treatment with CuPh, V449C-expressing oocytes still display glutamate-elicited currents that reverse near the oocyte chloride reversal potential. When DTT is added initially to reverse the spontaneous cross-links, the amplitude of glutamate-induced currents at −100 mV increases and the reversal potential becomes more positive compared to the untreated control (Fig. 7*A*). In addition, when the more permeable anion NO_3^- was substituted for chloride, we observed comparable glutamate-elicited currents in V449C-espressing oocytes after DTT or CuPh treatment (Fig. 7*B*). These results suggest that, remarkably, glutamate can still activate the anion conductance even when two subunits are constrained by cross-linking, and substrate transport no longer occurs.

Discussion

In contrast to the inward-facing crystal structure of Glt_{Ph}, which was captured by *intrasubunit* cross-linking (K55C and A364C), our work was driven by the observation that single cysteine substitutions for residues of HP2b in the human glutamate transporter EAAT1 form spontaneous and/or CuPh-catalyzed *intersubunit* cross-links (Fig. 1–3). Substrate translocation activity is abolished in the mutant transporters as a consequence of cross-linking, but the substrate-activated anion conductance associated with the carrier is retained (Fig. 7). The currently available outward- and inward-facing crystal structures of the Glt_{Ph} trimer would suggest that HP2b residues in adjacent subunits are too far to form disulfide bonds. Local movements of the HP2 loop, which have been visualized as an EC-gating mechanism in our recent MD simulations (14) and implied by the Glt_{Ph} structure bound with DL-threo-β-benzyloxyasparte (TBOA) (10), fall short of bringing two HP2b helices sufficiently close to form cross-links. ANM analysis, on the other hand, indicates two major types of large-scale motions that are energetically more favorable: an asymmetric stretching/contraction and a symmetric opening/closing of the three subunits (Movies S1–S3). Residues in the EC domains of adjacent subunits approach each other along both motions, and thus enable the formation of intersubunit disulfide bridges. In contrast, residues at the bottom of the transporter, within the membrane, remain rigid, in agreement with earlier findings (29). Cross-linking of cysteine substitutions at the N terminus of TM8 further supports the existence of large-scale intrinsic movements of subunits predicted by the ANM (Fig. 4*C*). Global motions of multimeric proteins are uniquely defined by their quaternary structures and are predicted to be similar with or without substrate bound (30). Indeed, there is also growing evidence for the functional relevance of global movements predicted by network models in substrate-free forms (23, 31). However, the local movements of HP2 also contribute to the HP2b cross-linking, because the binding of TBOA, which alters HP2 dynamics (13), can inhibit the formation of disulfide bridges (Fig. S8).

In contrast to our report, others have proposed that small-scale molecular motions of the core region are required for glutamate uptake in human glutamate transporters (32). Using FRET assays to determine the relative positions of EC residue pairs, Koch and Larsson observed no significant differences when comparing FRET efficiencies during transport and after transport is blocked by the removal of sodium. These findings can be easily reconciled with our observations. FRET assays determine the distance of residue pairs averaged over the experimental time frame of signal acquisition when proteins undergo a broad range of conformational fluctuations. Because the large collective motions proposed in our study are likely to occur in both substrate-free and actively translocating transporters, the average distances measured by FRET assays under the two conditions would be comparable.

In fact, such collective motions are essential to the transition from outward- to inward-facing state and vice versa, during the completion of the transport cycle. After cross-linking of V449C,

the un-cross-linked subunit is locked in an inwardly facing orientation, as evidenced by the inaccessibility from the EC environment of the V449C cysteine in the un-cross-linked subunit and the exposure of the L376C cysteine to the cytoplasm (Fig. 5). Thus, cross-linking captures a conformational state of EAATs in which two subunits of the trimer approach each other in the outward-facing state while the transport domain of the third subunit moves inward. These results suggest that the large changes in structure observed in our study could be functionally linked to the inward movement of the transport domain, a critical step for substrate transport.

ANM analysis confirms that the stepwise transition of individual subunits is a more viable mechanism to enable alternating access of the transporter, compared to an all-or-none transition of all three subunits. Earlier studies introduced mutations to alter the function of one or more subunits, determined their impact on overall function, and concluded that each subunit functions independently during transport (27, 28, 33). Although consistent with this idea, the experiments presented here, which disrupt the collective motions of the trimer, also reveal the higher-order cooperative nature of subunit–subunit interactions. Such cooperativity would not be captured in earlier studies because the mutations used would have no effect on global motions.

Remarkably, although the V449C mutant is unable to transport substrates after cross-linking, it retains substrate-elicited anion currents. We speculate that the un-cross-linked subunit in V449C is restricted in an inward-oriented conformation, which cannot be accessed by substrates to allow gating of the anion conductance. Thus, the glutamate-activated anion currents are generated by the two cross-linked subunits. Moreover, we previously showed that modification of V449C, which likely limits HP2 closure, also abolishes substrate transport, but increases the substrate-gated anion conductance (26). It is currently debatable which step in the substrate transport cycle conducts anion currents, but our results support the idea that a conducting state occurs at an early step after substrate binding.

Materials and Methods

Analyses of Substrate Transport and Transporter-Associated Currents in Mutant Carriers. Single cysteine residues were substituted in the cysteineless EAAT1 using site-directed mutagenesis (Stratagene). Glutamate uptake assays were performed in COS7 cells and *Xenopus* oocytes as described in figure legends. Two-electrode voltage clamp recordings were performed in EAAT-expressing oocytes using a Geneclamp 500B amplifier (Axon instruments) (26).

Detection of Transporter Proteins. Transporter proteins from ooctye membranes were prepared as described by Kobilka, with minor modifications (34). For thiol-specific biotinylation assays, cells were treated with maleimide-PEO_2-biotin (Thermo Scientific) or maleimide-biotin (Vector Labs) at 4 °C for 30 min, and biotinylated proteins were affinity purified with avidin beads. The protein samples were subjected to Western blotting analysis using a polyclonal antibody against the C terminus of EAAT1 (35).

Anisotropic Network Model Analysis. ANM analysis was performed as previously described with default parameters (22, 24). To model the intermediate states shown in Fig. 6, structures are constructed by assembling the individual inward- or outward-facing subunits upon superimposition of their N-terminal domains. The cumulative contribution of ANM modes to the transition between any pair of structures is described by cumulative overlap (25). Details of these methods can be found in the *SI Text*.

ACKNOWLEDGMENTS. The authors thank Bozena Kutyba-Brooks, Barbara Leighton, and Mary Skyba for excellent technical assistance in the early phase of this project. We also thank members of the Amara and Bahar laboratories for ongoing discussions and support. This work was supported by the National Institutes of Health Grants MH080726 (to S.G.A.) 1U54GM087519-01A1 (to I.B.), and R01-GM086328 (to I.B.).

1. Torres GE, Amara SG (2007) Glutamate and monoamine transporters: New visions of form and function. *Curr Opin Neurobiol* 17:304–312.
2. Zerangue N, Kavanaugh MP (1996) Flux coupling in a neuronal glutamate transporter. *Nature* 383:634–637.
3. Levy LM, et al. (1998) Inducible expression of the GLT-1 glutamate transporter in a CHO cell line selected for low endogenous glutamate uptake. *FEBS Lett* 422:339–342.
4. Fairman WA, Vandenberg RJ, Arriza JL, Kavanaugh MP, Amara SG (1995) An excitatory amino-acid transporter with properties of a ligand-gated chloride channel. *Nature* 375:599–603.
5. Wadiche JI, Amara SG, Kavanaugh MP (1995) Ion fluxes associated with excitatory amino acid transport. *Neuron* 15:721–728.
6. Veruki ML, Morkve SH, Hartveit E (2006) Activation of a presynaptic glutamate transporter regulates synaptic transmission through electrical signaling. *Nat Neurosci* 9:1388–1396.
7. Jardetzky O (1966) Simple allosteric model for membrane pumps. *Nature* 211:969–970.
8. Jiang J, Amara SG (2011) New views of glutamate transporter structure and function: Advances and challenges. *Neuropharmacology* 60:172–181.
9. Yernool D, Boudker O, Jin Y, Gouaux E (2004) Structure of a glutamate transporter homologue from Pyrococcus horikoshii. *Nature* 431:811–818.
10. Boudker O, Ryan RM, Yernool D, Shimamoto K, Gouaux E (2007) Coupling substrate and ion binding to extracellular gate of a sodium-dependent aspartate transporter. *Nature* 445:387–393.
11. Reyes N, Ginter C, Boudker O (2009) Transport mechanism of a bacterial homologue of glutamate transporters. *Nature* 462:880–885.
12. Leighton BH, Seal RP, Shimamoto K, Amara SG (2002) A hydrophobic domain in glutamate transporters forms an extracellular helix associated with the permeation pathway for substrates. *J Biol Chem* 277:29847–29855.
13. Grunewald M, Menaker D, Kanner BI (2002) Cysteine-scanning mutagenesis reveals a conformationally sensitive reentrant pore-loop in the glutamate transporter GLT-1. *J Biol Chem* 277:26074–26080.
14. Shrivastava IH, Jiang J, Amara SG, Bahar I (2008) Time-resolved mechanism of extracellular gate opening and substrate binding in a glutamate transporter. *J Biol Chem* 283:28680–28690.
15. Slotboom DJ, Sobczak I, Konings WN, Lolkema JS (1999) A conserved serine-rich stretch in the glutamate transporter family forms a substrate-sensitive reentrant loop. *Proc Natl Acad Sci USA* 96:14282–14287.
16. Shlaifer I, Kanner BI (2007) Conformationally sensitive reactivity to permeant sulfhydryl reagents of cysteine residues engineered into helical hairpin 1 of the glutamate transporter GLT-1. *Mol Pharmacol* 71:1341–1348.
17. Crisman TJ, Qu S, Kanner BI, Forrest LR (2009) Inward-facing conformation of glutamate transporters as revealed by their inverted-topology structural repeats. *Proc Natl Acad Sci USA* 106:20752–20757.
18. Leighton BH, Seal RP, Watts SD, Skyba MO, Amara SG (2006) Structural rearrangements at the translocation pore of the human glutamate transporter, EAAT1. *J Biol Chem* 281:29788–29796.
19. Ryan RM, Mitrovic AD, Vandenberg RJ (2004) The chloride permeation pathway of a glutamate transporter and its proximity to the glutamate translocation pathway. *J Biol Chem* 279:20742–20751.
20. Katz BA, Kossiakoff A (1986) The crystallographically determined structures of atypical strained disulfides engineered into subtilisin. *J Biol Chem* 261:15480–15485.
21. Falke JJ, et al. (1988) Structure of a bacterial sensory receptor. A site-directed sulfhydryl study. *J Biol Chem* 263:14850–14858.
22. Atilgan AR, et al. (2001) Anisotropy of fluctuation dynamics of proteins with an elastic network model. *Biophys J* 80:505–515.
23. Bahar I, Lezon TR, Bakan A, Shrivastava IH (2010) Normal mode analysis of biomolecular structures: Functional mechanisms of membrane proteins. *Chem Rev* 110:1463–1497.
24. Eyal E, Yang LW, Bahar I (2006) Anisotropic network model: Systematic evaluation and a new web interface. *Bioinformatics* 22:2619–2627.
25. Bahar I, Lezon TR, Yang LW, Eyal E (2010) Global dynamics of proteins: Bridging between structure and function. *Annu Rev Biophys* 39:23–42.
26. Seal RP, Shigeri Y, Eliasof S, Leighton BH, Amara SG (2001) Sulfhydryl modification of V449C in the glutamate transporter EAAT1 abolishes substrate transport but not the substrate-gated anion conductance. *Proc Natl Acad Sci USA* 98:15324–15329.
27. Grewer C, et al. (2005) Individual subunits of the glutamate transporter EAAC1 homotrimer function independently of each other. *Biochemistry (Mosc)* 44:11913–11923.
28. Koch HP, Brown RL, Larsson HP (2007) The glutamate-activated anion conductance in excitatory amino acid transporters is gated independently by the individual subunits. *J Neurosci* 27:2943–2947.
29. Groeneveld M, Slotboom DJ (2007) Rigidity of the subunit interfaces of the trimeric glutamate transporter GltT during translocation. *J Mol Biol* 372:565–570.
30. Bahar I, Chennubhotla C, Tobi D (2007) Intrinsic dynamics of enzymes in the unbound state and relation to allosteric regulation. *Curr Opin Struct Biol* 17:633–640.
31. Tobi D, Bahar I (2005) Structural changes involved in protein binding correlate with intrinsic motions of proteins in the unbound state. *Proc Natl Acad Sci USA* 102:18908–18913.
32. Koch HP, Larsson HP (2005) Small-scale molecular motions accomplish glutamate uptake in human glutamate transporters. *J Neurosci* 25:1730–1736.
33. Torres-Salazar D, Fahlke C (2006) Intersubunit interactions in EAAT4 glutamate transporters. *J Neurosci* 26:7513–7522.
34. Kobilka BK (1990) The role of cytosolic and membrane factors in processing of the human beta-2 adrenergic receptor following translocation and glycosylation in a cell-free system. *J Biol Chem* 265:7610–7618.
35. Seal RP, Leighton BH, Amara SG (1998) Transmembrane topology mapping using biotin-containing sulfhydryl reagents. *Methods Enzymol* 296:318–331.

Supporting Information

Jiang et al. 10.1073/pnas.1112216108

SI Material and Methods

Blue Native (BN) Polyacrylamide Gel Analysis. BN-PAGE was carried out as described (1). Protein samples were collected from oocytes and then homogenized in 500 μL of sucrose buffer (250 mM sucrose, 20 mM imidazole/HCl, pH 7.0). The samples were centrifuged for 10 min at 10,000 × *g* and the pellets were dissolved in 10% glycerol, 0.2% (wt/vol) Serva blue G, and 2% digitonin before applied onto gradient polyacrylamide gels. For SDS-PAGE, proteins were solubilized in 2% SDS and incubated at 56 °C for 1 h before electrophoresis.

Calculation of the Reaction Rate Constants. The reaction rate constants for copper phenanthroline (CuPh)-catalyzed cross-linking were determined by plotting the fraction of uptake remaining (F = uptake after/uptake before) as a function of the concentration of CuPh and then fit to a nonlinear regression equation for one phase exponential decay, $F = F_{\max} \times \exp^{(-yct)} - F_{\min}$, where t is the incubation time in seconds (5 min), c is the concentration of CuPh reagent, and y is the second-order reaction rate constant expressed as (M^{-1} s^{-1}).

Anisotropic Network Model (ANM) Analysis. ANM analysis is a coarse-grained normal mode analysis, which models the structure as an elastic network with individual nodes corresponding to the α-carbons of the protein. Interresidue interactions are described by harmonic potentials with uniform spring constant γ. For a protein of N residues, ANM predicts an ensemble of $3N$-6 modes of motion. The motion along mode k changes the position of residue i as (2)

$$\boldsymbol{R}_i^{(k)}(\pm S) = \boldsymbol{R}_i^{0} \pm S\lambda_k^{(-\frac{1}{2})}[\boldsymbol{u}_k]_i \qquad \text{[S1]}$$

where $\boldsymbol{R}_i^{0}$ is the position vector in the original (i.e., X-ray) structure, S is a parameter that scales the size of the deformation induced by mode k, $[\boldsymbol{u}_k]_i$ is the i^{th} superelement (three-dimensional vector) of the k^{th} eigenvector $\boldsymbol{u}_k$ (a $3N$-dimensional normalized vector) of the $3N \times 3N$ Hessian matrix $\mathbf{H}$, and λ_k is the corresponding eigenvalue (3, 4). The motion of residue i along the k^{th} principal/normal coordinate is described by $[\boldsymbol{u}_k]_i$, and $\lambda_k^{(-\frac{1}{2})}$ scales with the frequency of the k^{th} mode, such that lower-frequency modes make larger contributions to $\boldsymbol{R}_i^{(k)}$. The lowest frequency modes, also called the softest modes, define the mechanisms of global reconfiguration intrinsically favored by the molecular architecture under physiological conditions. Here we carried out the ANM with default parameters based on the Glt_{ph} outward-facing structure [Protein Data Bank (PDB) ID 1XFH], inward-facing structure (PDB ID 3KBC), and models constructed for intermediate states (see below).

Modeling the Structure and Dynamics of Intermediate States. Intermediate structures are constructed by assembling the individual inward- or outward-facing subunits upon superimposition of their trimerization domains. The difference between any pair of structures (including the experimentally observed all-outward or all-inward states, and the modeled/assembled intermediate states) is quantitatively described by a $3N$-dimensional deformation vector $\boldsymbol{d}$, evaluated by overlaying the two structures to remove rigid-body translations and rotations. The correlation between the k^{th} mode of motion predicted by the ANM and the deformation $\boldsymbol{d}$ is given by $\cos(\boldsymbol{u}_k,\boldsymbol{d}) = \boldsymbol{u}_k.\boldsymbol{d}/|\boldsymbol{d}|$ where $|\boldsymbol{d}|$ is the magnitude of $\boldsymbol{d}$, and $\boldsymbol{u}_k$ is the k^{th} eigenvector calculated for the starting structure. The *cumulative overlap* (Fig. 6 *C* and *D*) between a subset of soft modes (m of them) and the observed/modeled structural change $\boldsymbol{d}$ is given by

$$O_{\text{cum}}(m) = \left[\sum_{k=1}^{m} \cos^2(\boldsymbol{u}_k,\boldsymbol{d})\right]^{1/2}. \qquad \text{[S2]}$$

By definition, $O_{\text{cum}}(m)$ sums up to unity for $m = 3N$-6, because the $3N$-6 eigenvectors form an orthonormal basis set that spans the space of conformational changes. In the extreme case of completely random modes, which are uncorrelated with $\boldsymbol{d}$, $O_{\text{cum}}(m) = (m/3N\text{-}6)^{1/2}$. This relationship defines the control curves in Fig. 6 *C* and *D*. High cumulative overlaps achieved by a small subset of low-frequency modes indicate the accessibility of the structural changes via soft (energetically favorable) motions.

Data Analyses. Data were presented as Mean ± SEM and were analyzed using Student's t test. $P < 0.05$ was considered to be statistically significant.

1. Wittig I, Braun HP, Schagger H (2006) Blue native PAGE. *Nat Protoc* 1:418–428.
2. Xu C, Tobi D, Bahar I (2003) Allosteric changes in protein structure computed by a simple mechanical model: Hemoglobin $T \leftrightarrows R2$ transition. *J Mol Biol* 333:153–168.
3. Cui Q, Bahar I (2006) Normal mode analysis: Theory and applications to biological and chemical systems (Chapman & Hall, London).
4. Atilgan AR, et al. (2001) Anisotropy of fluctuation dynamics of proteins with an elastic network model. *Biophys J* 80:505–515.

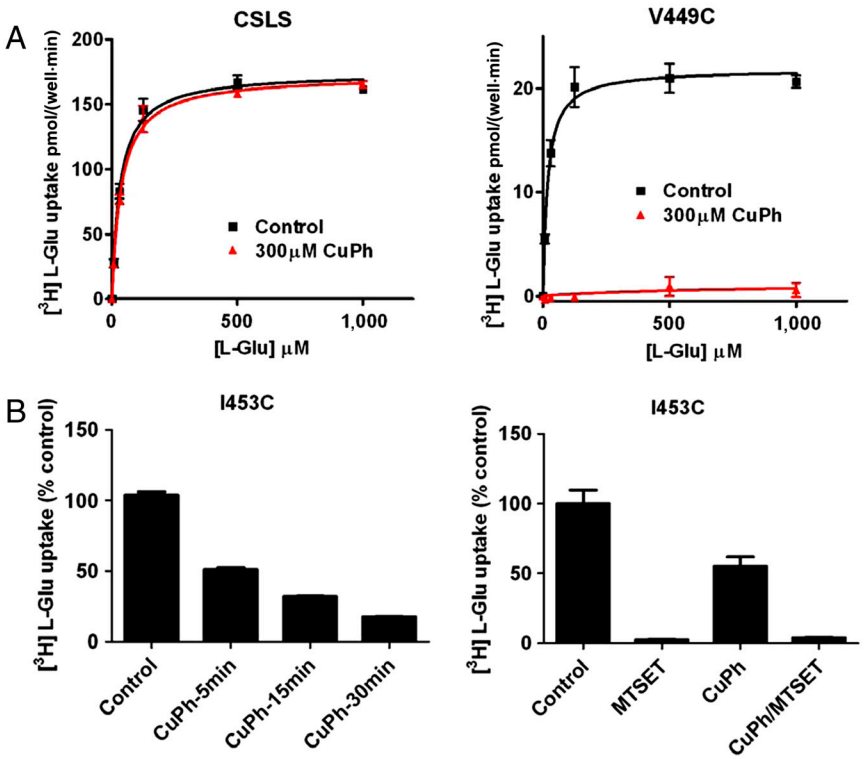

Fig. S1. (*A*) Five-minute incubation with 300 μM CuPh abolishes the substrate transport of V449C at both low and high (up to 1 mM) concentration of L-glutamate. CSLS, highly functional cysteineless version of human EAAT1 (excitatory amino acid transporter 1). (*B*) After 5-min incubation with 300 μM CuPh, the remaining substrate transport in the mutant I453C is due to incomplete cross-linking, because additional treatment with a thiol-modifying reagent, [2-(Trimethylammonium)ethyl] methanethiosulfonate bromide (MTSET), or prolonged incubation with CuPh further reduces its activity.

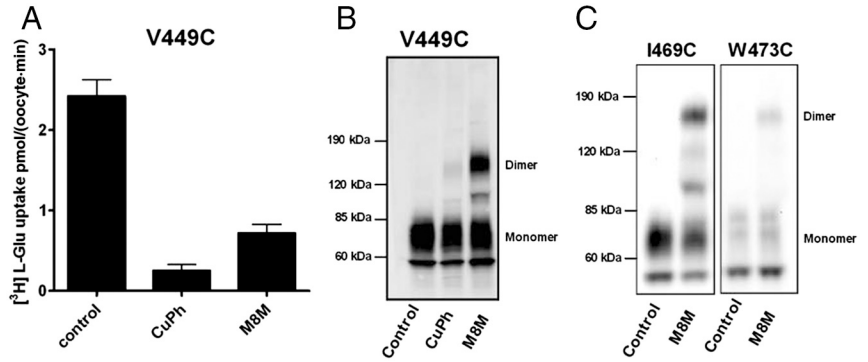

Fig. S2. The effect of a bifunctional sulfhydryl crosslinker, 1,8-octadiyl bismethanethiosulfonate (M8M), on the mutants V449C, I469C, and W473C. (*A*) M8M significantly inhibits the uptake activity of V449C. Oocytes expressing V449C were treated with 300 μM CuPh or 1 mM M8M for 5 min. Uptake assays were performed as described in Fig. 1. After indicated treatment, oocyte membrane samples were also collected and subjected to Western blotting analyses using an excitatory amino acid transporter 1 (EAAT1)-specific antibody. (*B*) M8M induces a prominent dimer species of the V449C mutant when analyzed by nonreducing SDS-PAGE. (*C*) M8M also cross-links I469C and W473C, because dimer species appear after M8M treatment when oocyte membrane proteins were separated by nonreducing SDS-PAGE.

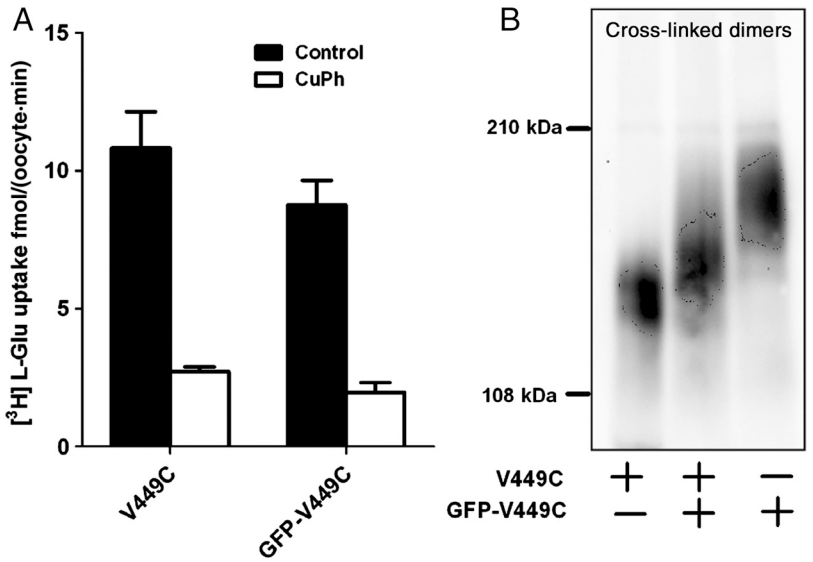

Fig. S3. CuPh-catalyzed V449C cross-links take place between two transporter subunits. (*A*) We constructed an N-terminus GFP-tagged V449C. When expressed in *Xenopus* oocytes, 5-min incubation with 300 μM CuPh significantly inhibits uptake activity of GFP-V449C, similar to that observed for nontagged V449C. (*B*) We expressed V449C, GFP-V449C, or a 1:1 ratio of V449C/GFP-V449C mixture in oocytes and treated the cells with 1 mM 1,8-octadiyl bismethanethiosulfonate (M8M) for 5 min, which induces stronger cross-linked dimer band signals on SDS gels. When membrane protein samples were separated by nonreducing SDS-PAGE, three different species of cross-linked dimers were detected, corresponding to V449C/V449C, V449C/GFP-V449C, and GFP-V449C/GFP-V449C. If the subunits were cross-linked to an unknown protein, we would expect to see two cross-linked species, one between V449C and the unknown protein, and the other between GFP-V449C and the unknown protein.

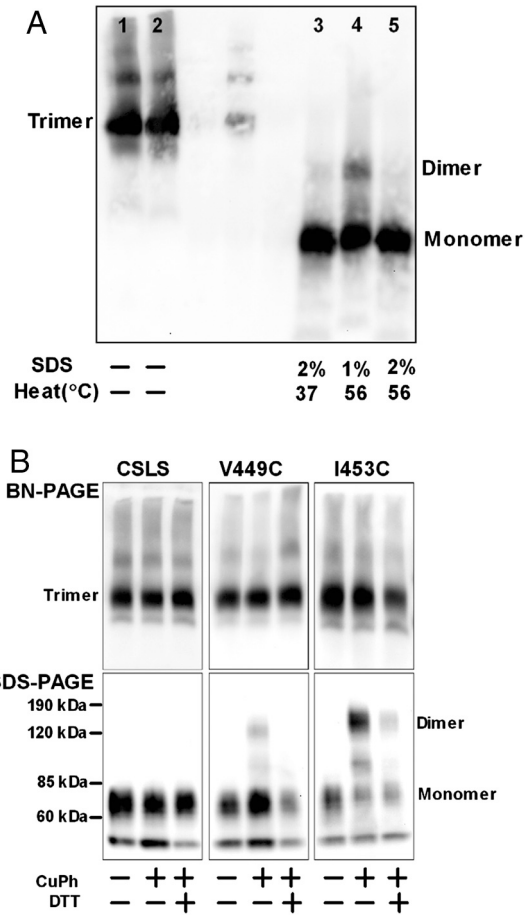

Fig. S4. CuPh-induced cross-links occur within a single excitatory amino acid transporter 1 (EAAT1) trimer. (*A*) Glutamate transporters migrate as trimers. Highly functional cysteineless version of human EAAT1 (CSLS) glutamate transporters were expressed in *Xenopus* oocytes. Oocyte membranes were collected for BN-PAGE analyses (left two lanes). The native samples were further treated with SDS and heat as indicated to dissociate the oligomer structure (right three lanes). The Western blot was probed with a C-terminally directed EAAT1-specific antibody. In lanes 1 and 2, the nondenatured unreduced CSLS EAAT1 migrates at a similar position as apoferritin (approximately 220 kDa), consistent with a trimeric EAAT structure. Lanes 3, 4, and 5 show the dissociation of the trimeric structure that occurs under different denaturing conditions (Lanes: 3, 37 °C/2% SDS; 4, 56 °C/1% SDS; and 5: 56 °C/2% SDS). (*B*) CuPh-induced cross-links occur within a single EAAT1 trimer. CSLS and cysteine-substituted transporters were expressed in *Xenopus* oocytes. Oocytes were treated with 300 μM CuPh, or 300 μM CuPh followed by 20 mM DTT, for 5 min. Oocyte membranes were collected for BN-PAGE analysis. If the cross-links were intertrimeric, we would expect to see the cross-linked transporters migrate at minimum as a hexamer. The mutants V449C and I453C display trimer species of similar intensity before and after treatment with 300 μM CuPh and no higher molecular weight cross-linked species are observed (*Upper*). The native samples were further incubated at 56 °C for 1 h in the presence of 2% SDS, which completely disrupted trimeric CSLS transporters to monomers. After CuPh treatment, V449C and I453C display dimer bands in addition to their monomer (*Lower*).

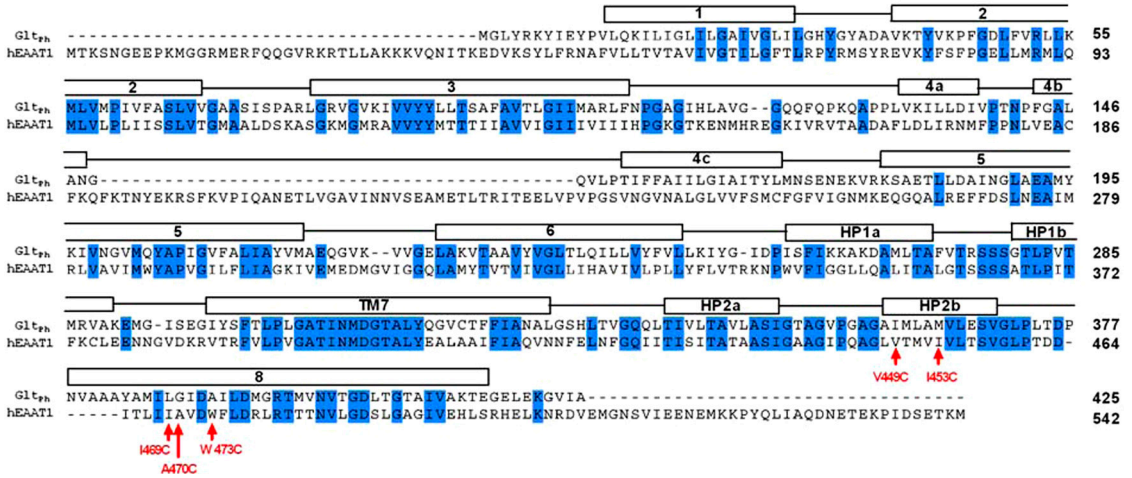

Fig. S5. Sequence alignment of Glt_{Ph} and human excitatory amino acid transporter 1 (EAAT1). Boxes above the alignment correspond to transmembrane (TM) domains and sequences highlighted in blue are regions of exact identity between the two carriers. The mutants used for experiments are indicated with red arrows [V449C and I453C in helical hairpin 2 (HP2) region, and the mutants I469C, A470C and W473C in TM8]. The alignment was made using ClustalW and adjusted manually. Sequences used in the alignment are *Pyrococcus horikoshii* Glt_{Ph} (PubMed ID NP_143181) and human EAAT1 (P43003).

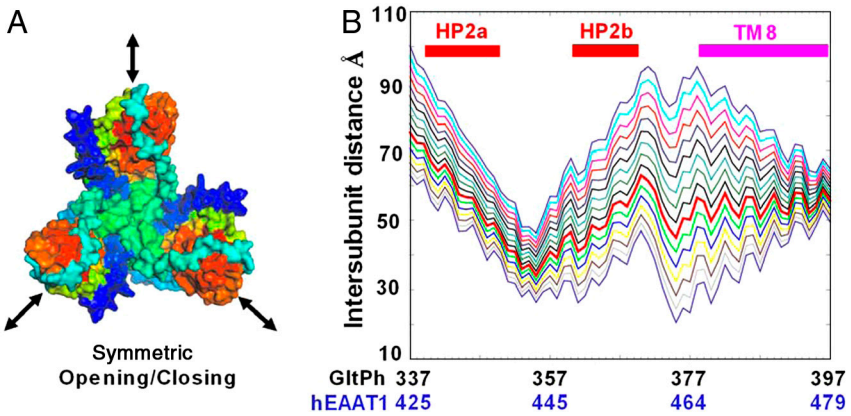

Fig. S6. Symmetric opening/closing movement of glutamate transporters predicted by ANM analysis. (*A*) Schematic representation of the symmetric opening/closing mode viewed from the extracellular face. The arrows indicate the direction of motion of the three subunits. (*B*) The distances of residues (C^{α} atoms) in helical hairpin 2 (HP2) and transmembrane 8 (TM8) between two approaching subunits are significantly altered along the symmetric opening/closing mode. The thick red curve refers to the equilibrium distances (in the X-ray structure), and the series of curves above and below refer to different extents of deformation along this mode in the positive and negative directions. The corresponding excitatory amino acid transporter 1 (EAAT1) residues are denoted in blue, below the abscissa.

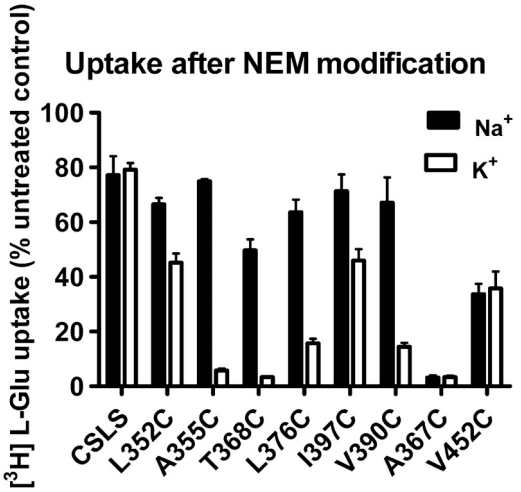

Fig. S7. Inhibition of substrate transport in single cysteine mutants by *N*-ethylmaleimide (NEM) in the presence of either sodium or potassium. The alternating access model predicts that distinct sets of residues are exposed to the intracellular environment depending upon whether the carrier faces inwardly or outwardly. Several cysteine mutants in transmembrane 7 and helical hairpin 1 display increased accessibility to NEM when external sodium was replaced by potassium, a condition expected to increase the proportion of inward-facing transporters. Bars in the figure indicate the percent of activity remaining for each mutant in sodium—or potassium—containing solution, and treated with or without NEM. The concentration of NEM used was 0.25 mM, except for the mutant L352C where 1 mM NEM was used. These results confirm that residues A355C, T368C, L376C, and V390C are conformation sensitive and show increased intracellular exposure as the transport domain moves toward the cytoplasm.

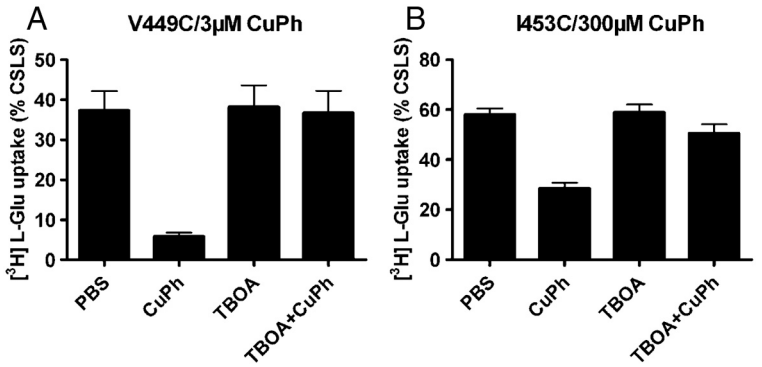

Fig. S8. DL-threo-β-benzyloxyasparte (TBOA) protects the cross-linking of V449C and I453C by CuPh. TBOA (150 μM) was added during a 5-min treatment with CuPh before uptake assay. (*A*) Lower concentrations of CuPh (3 μM) is used to cross-link V449C. (*B*) CuPh (300 μM) is used to cross-link I453C. CSLS, highly functional cysteineless version of human excitatory amino acid transporter 1.

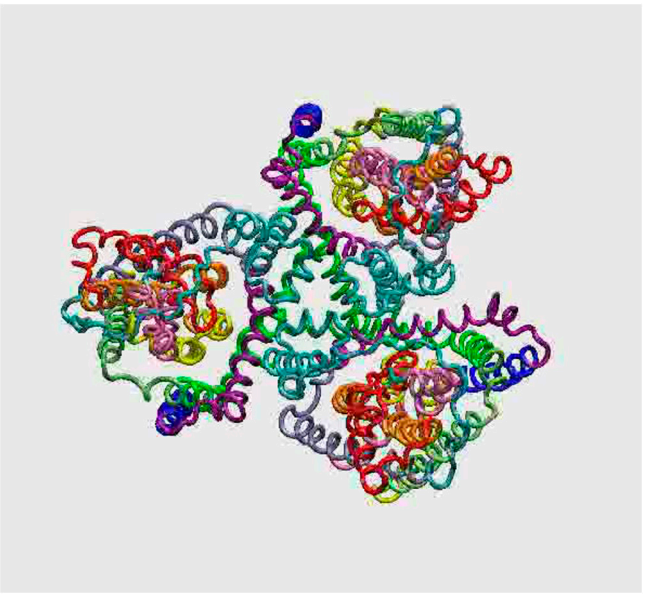

Movie S1. Movie illustrating the motion of the outward-facing glutamate transporter trimer in ANM mode 1 (softest mode). In this mode, two subunits come close together while the third moves away from the other two. This mode is degenerate with mode 2 (they have same eigenvalues).

Movie S1 (MPG)

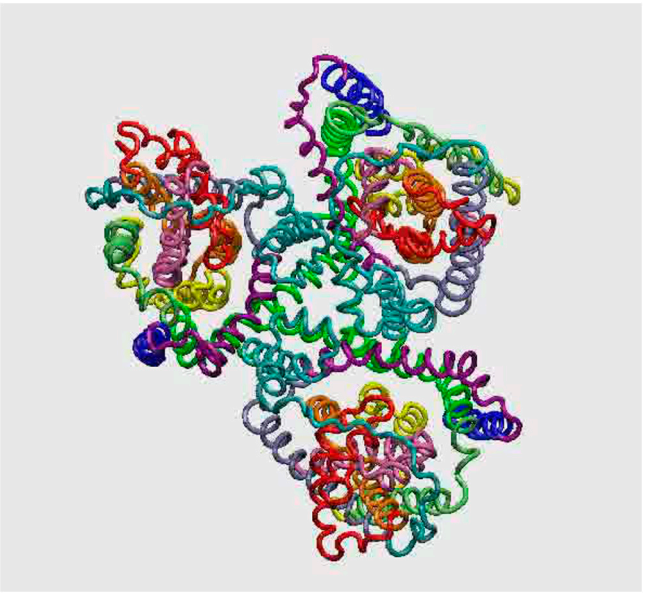

Movie S2. Movie illustrating the motion of the outward-facing glutamate transporter in ANM mode 2. This mode is similar to mode 1 except that the pair of approaching subunits is different.

Movie S2 (MPG)

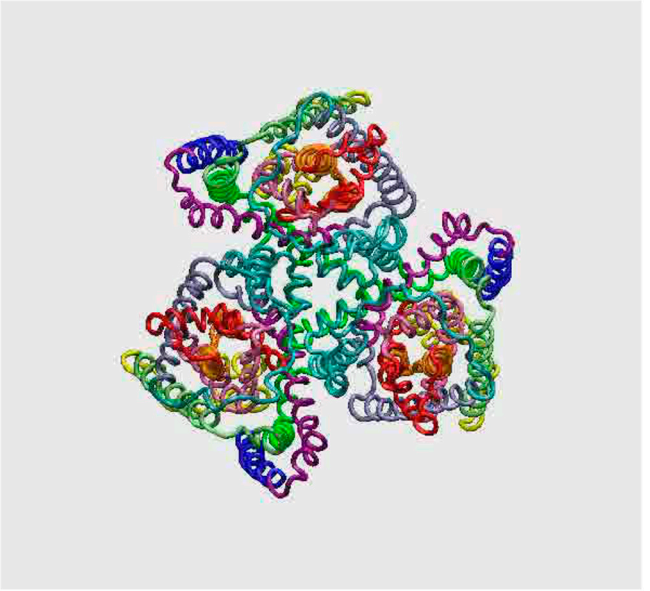

Movie S3. Movie illustrating the motion of the outward-facing transporter in ANM mode 3. In this symmetric mode, all three subunits move simultaneously toward or away from each other over the aqueous basin.

Movie S3 (MPG)